QUARTERLY TECHNICAL PROGRESS REPORT
FOR THE PERIOD ENDING MARCH 31, 2007

TITLE: ANALYSIS OF CRITICAL PERMEABLITY, CAPILLARY PRESSURE AND ELECTRICAL PROPERTIES FOR MESAVERDE TIGHT GAS SANDSTONES FROM WESTERN U.S. BASINS

DOE Contract No. DE-FC26-05NT42660

Contractor:	University of Kansas Center for Research, Inc. 2385 Irving Hill Road Lawrence, KS 66044
DOE Program:	Natural Gas Technologies (Advanced Diagnostics & Imaging)
Award Date:	October 1, 2005
Total Project Budget:	$513,834
DOE Cost Amount:	$411,030
Program Period:	October 1, 2005 – September 30, 2007
Reporting Period:	January 1, 2007 – March 31, 2007
DOE Project Manager:	Purna Halder, NETL Tulsa, OK
Contractor Contact:	Alan P. Byrnes Kansas Geological Survey 1930 Constant Ave., Lawrence, Kansas 66047 email: abyrnes@kgs.ku.edu phone: 785-864-2177
Principal Investigators:	Alan P. Byrnes (Program Manager) Robert Cluff (Discovery Group) John Webb (Discovery group)

DISCLAIMER:

ABSTRACT:

Mercury intrusion capillary pressure (MICP) analysis from 2 to 9,300 psi injection pressure for unconfined samples are complete for 145 samples and confined mercury intrusion analyses are complete for 85 samples. For the unconfined samples 32 were selected for hysteresis analysis involving three drainage-imbibition cycles for each sample. These three cycles represent drainage saturations reaching successively Snw = 0.33$\pm$0.15, Snw = 0.57$\pm$0.10, and Snw 0.87$\pm$0.10. Analysis of residual mercury (nonwetting phase) saturations for these measurements and for the single-maximum nonwetting phase saturation of the remaining unconfined samples and the high-pressure confined samples indicates that residual nonwetting phase saturation (Snwr) can be predicted from initial nonwetting phase saturation (Snwi) within an accuracy of $\pm$0.07 (1 standard deviation) using the Land relation: 1/Snwr-1/Snwi = C where C = 0.55. Predicted Snwr is relatively insensitive to variance in the value of C near this value. Analysis of previously reported C = 0.8$\pm$0.2, based on the average of individual sample C values, indicates that this value is accurate for the average but does not provide the minimum error of prediction for all samples combined.

Pore volume compressibility measurements on 113 samples for confining pressures from 200 to 4000 psi (1.4-27.6 MPa) indicate that pore volume compressibility can be predicted for any given Mesaverde low-permeability sandstone with a given porosity at any given net effective confining pressure using:

$\beta = 10^{\wedge}[(0.000031\phi^2+0.00275\phi-1.016)*\log_{10}P+(0.000034\phi^3-0.00223\phi^2+0.056\phi+4.238)]$

Where β is the pore volume compressibility (10^{-6}/psi), P is the average net effective confining pressure (psi) at which β applies, and ϕ is the unconfined routine porosity (%).From this equation compressibility can be seen to change with sandstone porosity and the net effective stress.

TABLE OF CONTENTS

LIST OF TABLES

LIST OF FIGURES

Acronyms

C = Land equation constant
Hg = mercury
k_{ik} = *in situ* Klinkenberg permeability, millidarcies
md = mD = millidarcy, 1 md = 9.87×10^{-4} μm^2
MICP = mercury intrusion capillary pressure
psi = pound per square inch, 1 psi = 6.89 kPa = 0.00689 MPa
Snwi = initial nonwetting phase saturation
Snwr = residual nonwetting phase saturation
Swirr = "irreducible" wetting phase saturation
β = pore volume compressibility (10^{-6}/psi)
P = average net effective confining pressure (psi)
ϕ = porosity, percent or fraction depending on context

INTRODUCTION

Objectives - Industry assessment of the regional gas resource, projection of future gas supply, and exploration programs require an understanding of the reservoir properties and accurate tools for formation evaluation of drilled wells. The goal of this project is to provide petrophysical formation evaluation tools related to relative permeability, capillary pressure, electrical properties and algorithm tools for wireline log analysis. Major aspects of the proposed study involve a series of tasks to measure drainage critical gas saturation, capillary pressure, electrical properties and how these change with basic properties such as porosity, permeability, and lithofacies for tight gas sandstones of the Mesaverde Group from six major Tight Gas Sandstone basins (Washakie, Uinta, Piceance, Upper Greater Green River, Sand Wash and Wind River). Critical gas saturation (Sgc) and ambient and *in situ* capillary pressure (Pc) will be performed on 150 rocks selected to represent the range of lithofacies, porosity and permeability in the Mesaverde.

Project Task Overview -

Task 1. Research Management Plan
Task 2. Technology Status Assessment
Task 3. Acquire Data and Materials
- Subtask 3.1. Compile published advanced properties data
- Subtask 3.2. Compile representative lithofacies core and logs from major basins
- Subtask 3.3. Acquire logs from sample wells and digitize

Task 4. Measure Rock Properties
- Subtask 4.1. Measure basic properties (k, ϕ, grain density) and select advanced population
- Subtask 4.2. Measure critical gas saturation
- Subtask 4.3. Measure in situ and routine capillary pressure
- Subtask 4.4. Measure electrical properties
- Subtask 4.5. Measure geologic and petrologic properties
- Subtask 4.6. Perform standard logs analysis

Task 5. Build Database and Web-based Rock Catalog
- Subtask 5.1. Compile published and measured data into Oracle database
- Subtask 5.2. Modify existing web-based software to provide GUI data access

Task 6. Analyze Wireline-log Signature and Analysis Algorithms
- Subtask 6.1. Compare log and core properties
- Subtask 6.2. Evaluate results and determine log-analysis algorithm inputs

Task 7. Simulate Scale-dependence of Relative Permeability
- Subtask 7.1. Construct basic bedform architecture simulation models
- Subtask 7.2. Perform numerical simulation of flow for basic bedform architectures

Task 8. Technology Transfer, Reporting, and Project Management
- Subtask 8.1 Technology Transfer
- Subtask 8.2. Reporting Requirements
- Subtask 8.3. Project Management

EXECUTIVE SUMMARY:

Mercury intrusion capillary pressure (MICP) analysis from 2 to 9,300 psi injection pressure for unconfined samples are complete for 145 samples and confined mercury intrusion analyses are complete for 85 samples. For the unconfined samples 32 were selected for hysteresis analysis involving three drainage-imbibition cycles for each sample. Analysis of residual mercury (nonwetting phase) saturations for these measurements and for the single-maximum nonwetting phase saturation of the remaining unconfined samples and the high-pressure confined samples indicates that Snwr can be predicted from Snwi within an accuracy of $\pm$0.07 (1 standard deviation) using the Land relation: 1/Snwr-1/Snwi = C where C = 0.55. Predicted Snwr is relatively insensitive to variance in the value of C near this value. Pore volume compressibility measurements on 113 samples for confining pressures from 200 to 4000 psi (1.4-27.6 MPa) indicate that pore volume compressibility can be predicted for any given Mesaverde low-permeability sandstone with a given porosity at any given net effective confining pressure using:

$\beta = 10^{[(0.000031\phi^2+0.00275\phi-1.016)*\log_{10}P+(0.000034\phi^3-0.00223\phi^2+0.056\phi+4.238)]}$

Where β is the pore volume compressibility (10^{-6}/psi), P is the average net effective confining pressure (psi) at which β applies, and ϕ is the unconfined routine porosity (%).

RESULTS AND DISCUSSION:

TASK 4. MEASURE ROCK PROPERTIES

Subtask 4.3. Measure *in situ* and routine capillary pressure

Mercury intrusion capillary pressure (MICP) analysis from 2 to 9,300 psi injection pressure for unconfined samples are complete for 145 samples and confined mercury intrusion analyses are complete for 85 samples. For the unconfined samples 32 were selected for hysteresis analysis involving three drainage-imbibition cycles for each sample. These three cycles represent drainage saturations reaching successively Snw = 0.33$\pm$0.15, Snw = 0.57$\pm$0.10, and Snw 0.87$\pm$0.10. Figure 1 illustrates representative hysteresis curves for sandstones exhibiting a range of permeabilities. As with other samples analyzed, a significant fraction of the trapped non-wetting phase saturation (Snw) results from the early intrusion at low Snw values. Figure 2 illustrates the relationship between the residual saturation to imbibition and the initial drainage saturation for each cycle. In addition to residual saturation measurements on the 32 hysteresis samples, all MICP samples were weighed following analysis. Residual mercury trapped in the core was determined gravimetrically and residual non-wetting phase saturation calculated. For these samples the initial mercury (nonwetting phase) saturation represented the mercury saturation achieved at 9,300 psi intrusion pressure. This saturation is near, or represents a wetting phase saturation less than, “irreducible” saturation. Figure 3 illustrates the relationship between residual nonwetting phase saturation and the initial nonwetting phase saturation for the hysteresis and the single-cycle unconfined MICP samples. The relationship between initial and residual nonwetting phase saturation was characterized by Land (1971) for strongly wet samples:

$$1/Snwr^* - 1/Snwi^* = C \qquad (1)$$

Where Snwr* = Snwr/(1-Swirr) and Snwi* = Snwi/(1-Swirr).

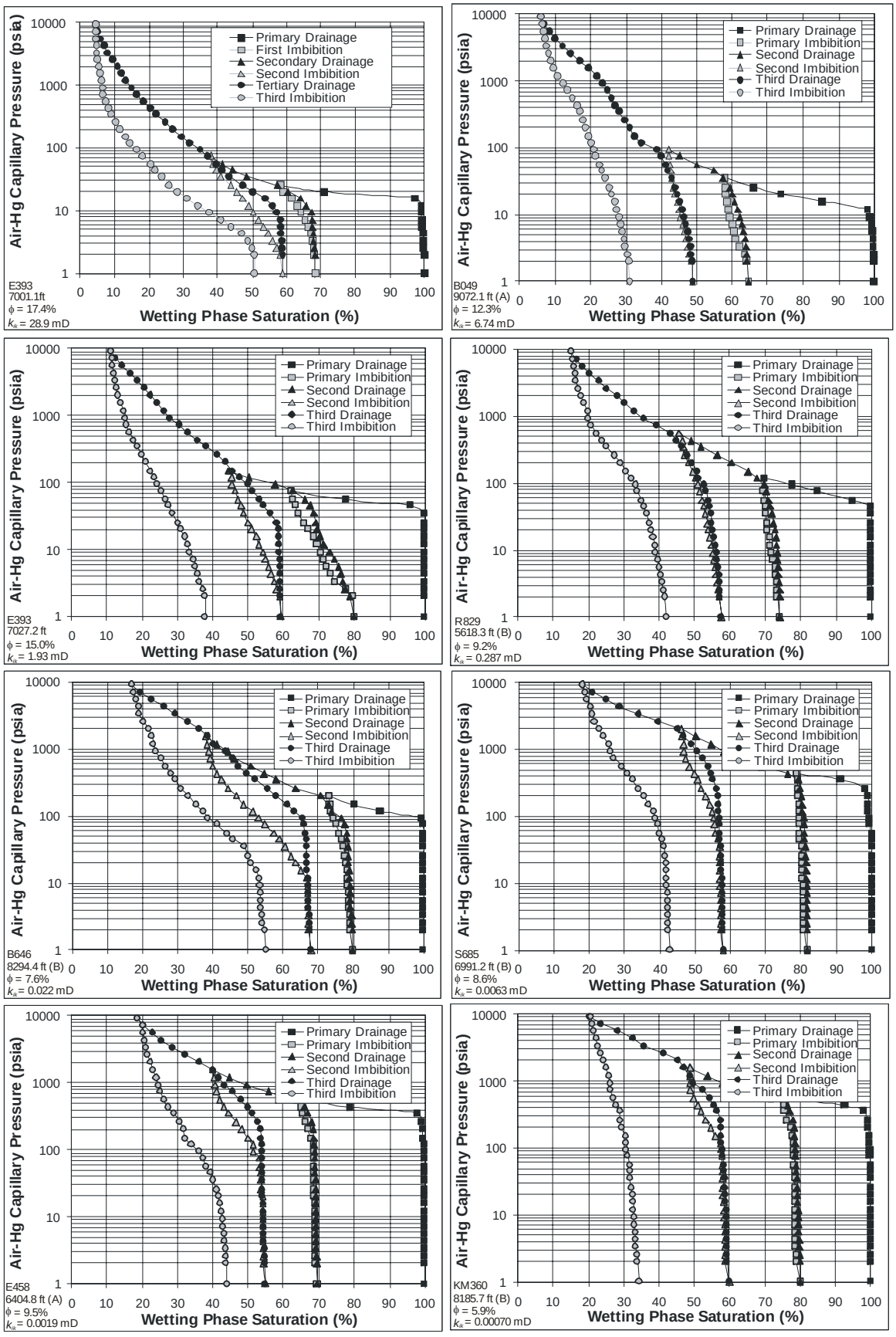

Figure 1. Example air-mercury successive drainage and imbibition capillary pressure curves

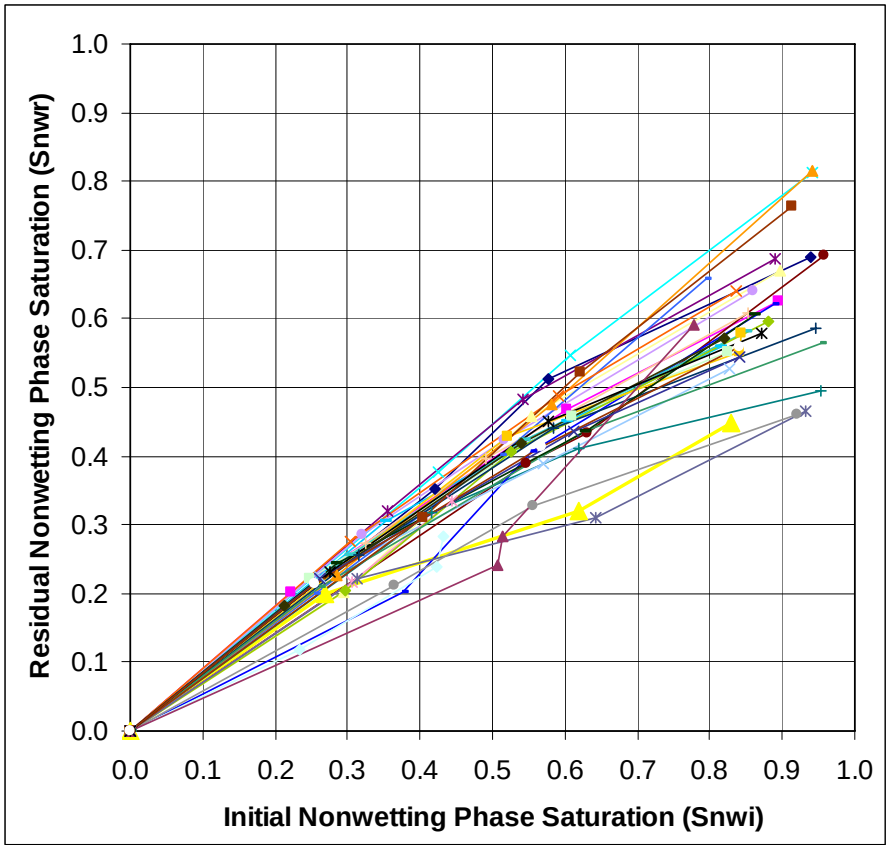

Figure 2. Crossplot of residual versus initial mercury (nonwetting) saturation for 32 Mesaverde sandstone samples.

Three different measurement populations are compared; unconfined, unconfined with hysteresis, and confined. Unconfined with hysteresis are separated from the unconfined because the hysteresis samples have data for measurements at Sw < Swirr except for the third and last hysteresis drainage-imbibition cycle. Confined samples are samples for which capillary pressure analysis was performed with the sample under a net confining stress of 4,000 psi (27.5 MPa) as described in previous reports. Table 1 compares Land C values for the different sample populations with Swirr defined as either equal to the minimum saturation achieved in the MICP analysis (Swirr = 1-Snwmax) or Swirr equal to zero (Swirr = 0). The average Land C values represent the average of individual C values calculated for each sample using equal 1. The Land C Minimum Error values represent the C values that provide a minimum error for all samples in a given population using a single C value.

Sample Condition	Swirr definition	Land C Average	C Standard Error	Land C Minimum Error	Snwr Standard Error	Snwr Std Error C=0.55
all	$S_{wirr} = 1-S_{nwmax}$	0.57	0.329	0.53	0.077	0.077
unconfined	$S_{wirr} = 1-S_{nwmax}$	0.61	0.294	0.59	0.087	0.088
hysteresis	$S_{wirr} = 1-S_{nwmax}$	0.61	0.383	0.51	0.056	0.057
confined	$S_{wirr} = 1-S_{nwmax}$	0.44	0.249	0.45	0.088	0.085
all	$S_{wirr} = 0$	0.73	0.443	0.63	0.073	0.073
unconfined	$S_{wirr} = 0$	0.78	0.360	0.71	0.080	0.081
hysteresis	$S_{wirr} = 0$	0.75	0.562	0.59	0.057	0.057
confined	$S_{wirr} = 0$	0.61	0.316	0.54	0.078	0.078
all	$S_{wirr} = 0$, Snwi<70%			0.70	0.054	0.053
unconfined	$S_{wirr} = 0$, Snwi<70%			0.83	0.062	0.061
hysteresis	$S_{wirr} = 0$, Snwi<70%			0.70	0.052	0.051
confined	$S_{wirr} = 0$, Snwi<70%			0.50	0.038	0.039

Table 1. Comparison of average Land C values for different sample populations calculated from averaging individual sample C values and from solution of the minimum error for each a single C value for each population.

Average C values, calculated from the average of the individual sample C values using equation 1 (with Swirr = 1-Swmin and Swirr = 0) average 0.07 greater than minimum error C values. Variance of the individually determined C values is significant, averaging 0.37. Land C values that result in the minimum error for a given population average 0.61±0.20 for all populations and 0.65±0.20 for the populations where Swirr = 0. Standard error is greater for Swirr = 1 –Snwmax than for Swirr = 0 even with input of individual known sample Swirr values. This argues that optimum prediction of Swnr is obtained using Swirr = 0. Although the Land C values appear to vary widely, resulting predicted residual saturation values are not highly sensitive for the range of C values exhibited. Iterative solution indicates that C = 0.55 results in the minimum error in residual saturation for all populations with Swirr = 0. Using C = 0.55 the resulting error in Snwr prediction is only 0.001±0.0015 different from the standard error values obtained using C value that provide the minimum error for each population (Table 1). Figure 3 illustrates initial (Snwi) and residual nonwetting phase saturations (Snwr) for the unconfined MICP samples, for which Snwi = 1- Snwmax, and the unconfined hysteresis samples, for which 2 of 3 Snwi< 1- Snwmax. Trapping is slightly greater in the hysteresis samples.

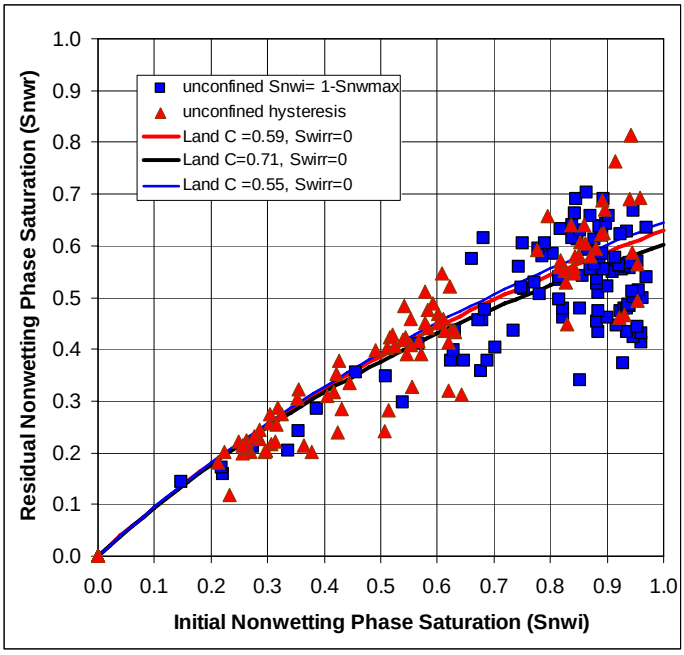

Figure 3. Crossplot of residual and initial nonwetting phase saturation for unconfined samples including samples where Snwi = 1 Snwmax (blue squares) and hysteresis/imbibition samples where 2 of 3 measurements were obtained at Snwi < 1 – Snwmax (red triangle).

Comparing the residual and initial saturations for unconfined and confined samples (Figure 4) shows that confined samples exhibit greater residual saturation than unconfined with C = 0.54 and C = 0.66 for confined and unconfined (including unconfined and unconfined hysteresis samples), respectively. Greater trapping in confined samples may be the result of a change in the pore body – pore throat relationship due to confining stress or it may be the result of the limit placed on exit boundary conditions. Unconfined samples allow mercury to exit the sample from all sides whereas confined samples only allow mercury to exit from one entry face. Assuming a constant number of exit paths in any given direction and the same snap-off conditions, a decrease in the number of exit paths is likely to increase the nonwetting phase volume behind junctions undergoing snap-off in one direction. This change in boundary conditions would likely result in some additional trapping. Whether the increase in residual nonwetting phase saturation is the result of confining stress effects or the difference in boundary conditions is being investigated.

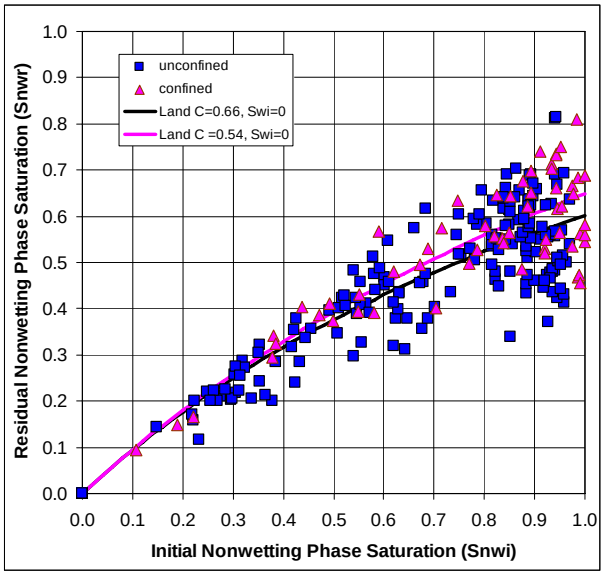

Figure 4. Crossplot of residual and initial nonwetting phase saturation for unconfined samples (blue squares) and confined samples (magenta triangles). Higher Snwr values in confined samples result in slightly greater Land C value. Whether increased trapping is due to confining stress effects or boundary conditions is still being investigated.

Based on analysis of prediction error for the confined and unconfined sample populations, prediction of Snwr using C = 0.55 and Swirr = 0 appears to provide minimum error for the range of possible measurement condition populations. Utilization of C values specific for a population results in improvement in prediction that is generally less than 2% of Snwr.

Subtask 4.3. Measure Electrical Properties

Given the change in pore structure exhibited by low-permeability sandstone permeability under confining stress and limited published data on the change in porosity with confining stress, it is important to measure electrical properties under confining stress. As previously reported electrical properties were measured with core under a hydrostatic confining stress of 4,000 psi (27.5 MPa). To better understand how pore volume changes with confining stress, pore volume compressibility measurements were performed on 113 representative samples. To measure *in situ* porosity the cores were evacuated for a period of eight (8) hours and then saturated with a deaerated 200,000 parts per million by weight sodium chloride (ppmw NaCl) brine solution. After vacuum saturation, complete saturation was obtained by applying a pressure of 1,000 psi (7 MPa) for a period of 24 hours to the saturating brine and samples. Complete saturation was confirmed by agreement between helium-measured porosity and gravimetric-saturation porosity values within 0.1 porosity percent. After the cores had reached equilibrium with the brine, each was placed in a biaxial Hassler-type core holder and subjected to a series of increasing hydrostatic confining stresses of 200, 400, 1000, 2000 and 4000 psi (1.4-27.6 MPa) approximating a range of reservoir stress conditions. For the apparatus utilized the porosity change from unconfined conditions to the first confining pressure of 200 psi could not be measured because the confining sleeve had to be "set" around the sample. This pressure varies with core diameter and surface roughness. Calibration measurements indicate that the sleeve is set for most regular core samples with diameter of 0.97-1.00 inches (0.0246-0.0254 m) at 50 $\pm$ 25 psi (345 $\pm$ 172 kPa). Pore volume decrease was determined by measuring the brine displaced from the core by compression using a micropipette, correcting for system compressibility changes. Pore pressure was at atmospheric pressure. Porosity calculations were performed assuming that the grains of the rock were incompressible and hence the bulk volume

decreased by the same amount as the pore volume. Equilibrium at pressure was assumed if pore volume change was less than 0.001 cc for a ten (10) minute period.

Figure 5 illustrates the pore volume change from 200 psi (1380 kPa) initial confining pressure with increasing confining stress for all samples. Every sample exhibited a log-linear relationship between the fraction of initial pore volume (pore volume at 200 psi confining pressure) at confining stress and the confining stress. The average correlation coefficient of the log-linear relationships is 0.99±0.031 (error range is 2 standard deviations).

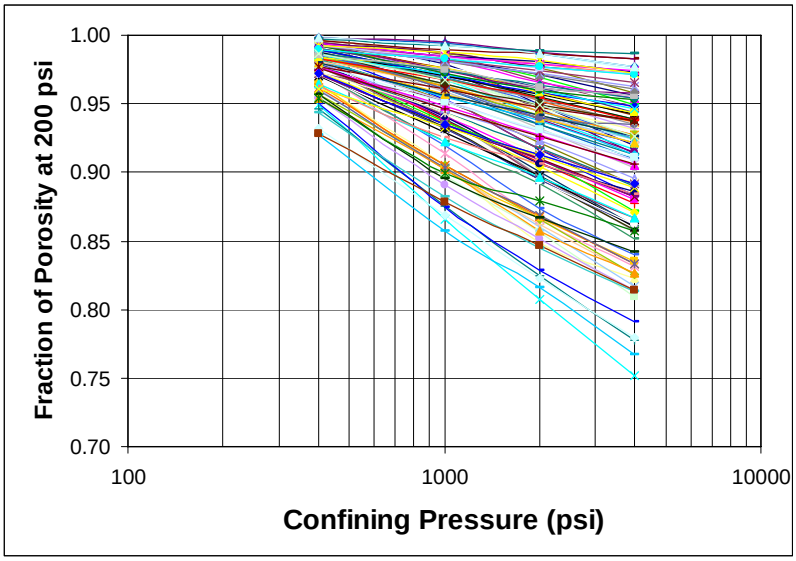

Figure 5. Crossplot of fraction of pore volume at 200 psi confining stress versus confining stress for all 113 samples. Every sample exhibits a log-linear relationship though slopes and intercepts differ.

This log-linear nature of the pore volume change has been previously shown in low-permeability sandstones to characterize crack or sheet-like pore volume compression (Ostensen, 1983). Slopes and intercepts of the curves in Figure 5 both increase with increasing porosity (Figure 6 and 7).

Figure 6. Crossplot of slope of log-linear curves in Figure 5 with porosity. The relationship between the slope and porosity can be expressed:

Slope = -(0.0060 ϕ + 0.03)

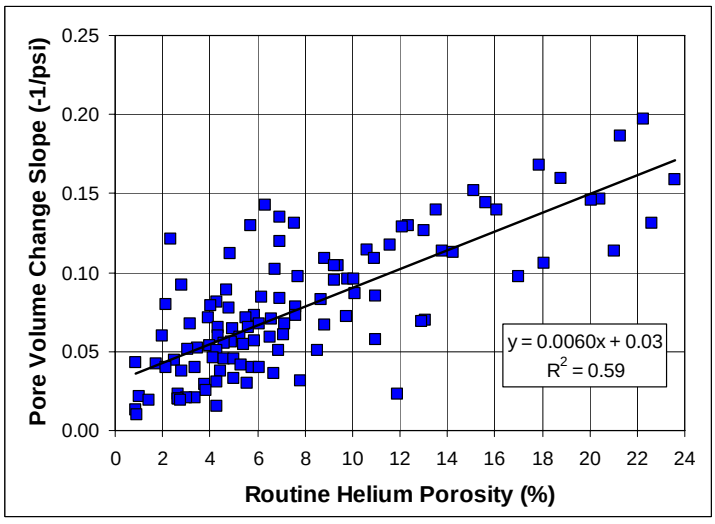

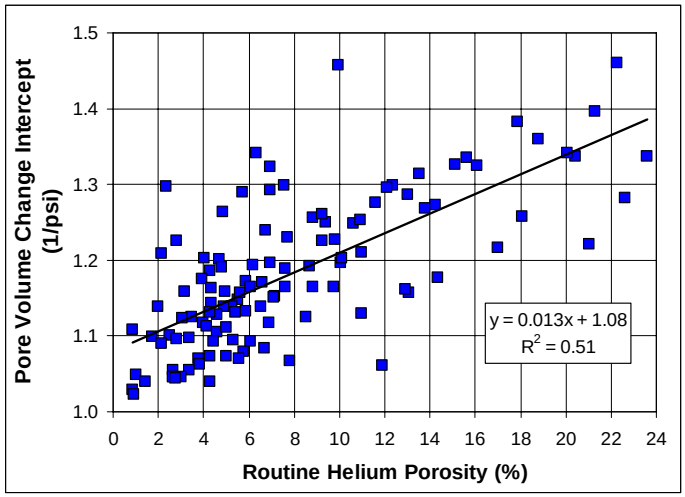

Figure 7. Crossplot of intercept of log-linear curves in Figure 5 with porosity. The relationship between the intercept and porosity can be expressed:

Intercept = 0.013 ϕ + 1.08

Utilizing the equations shown in Figures 6 and 7 to calculate slopes and intercepts for rocks of different porosity, the fraction of initial pore volume relationship can be transformed to pore volume compressibility (change in volume/ unit volume/ change in pressure; 1/psi). Figures 8 and 9 shown the slope and intercept relationships for prediction of pore volume compressibility of low-permeability sandstones that conform to the equations in Figures 6 and 7.

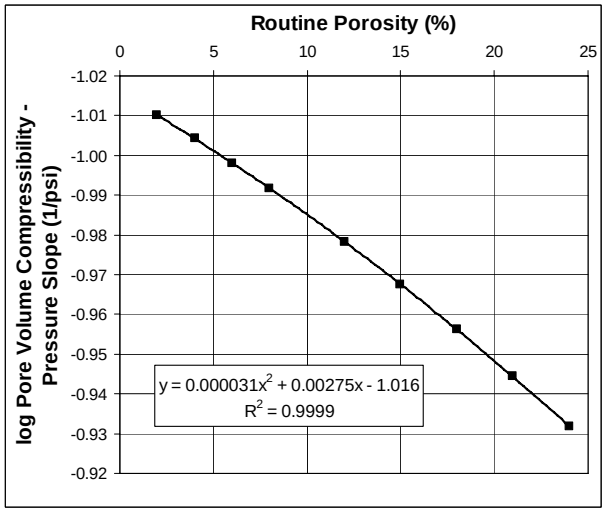

Figure 8. Crossplot of pore volume compressibility slope function versus porosity.

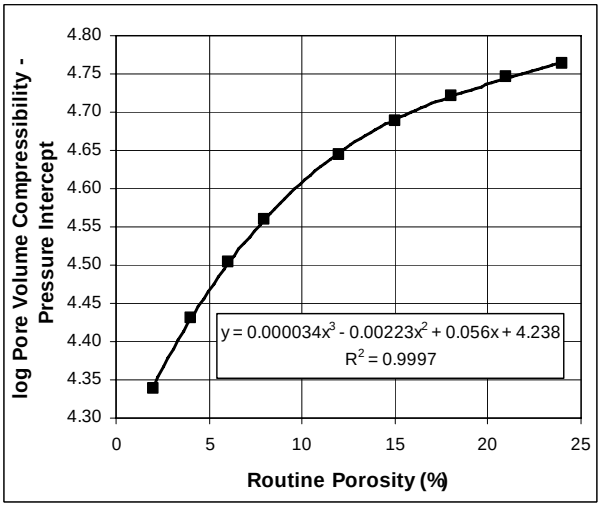

Figure 9. Crossplot of pore volume compressibility intercept function versus porosity.

Combining equations, pore volume compressibility can be predicted for any given Mesaverde low-permeability sandstone with a given porosity at any given net effective confining pressure using:

$$\beta = 10^{[(0.000031\phi^2+0.00275\phi-1.016)*\log_{10}P+(0.000034\phi^3-0.00223\phi^2+0.056\phi+4.238)]} \quad (2)$$

Where β is the pore volume compressibility (10^{-6}/psi), P is the average net effective confining pressure at which β applies, and ϕ is the unconfined routine porosity (%). Using equation 2 it is

evident that compressibility changes with sandstone porosity and the net effective stress. Figure 10 illustrates general compressibility curves for different porosity sandstones.

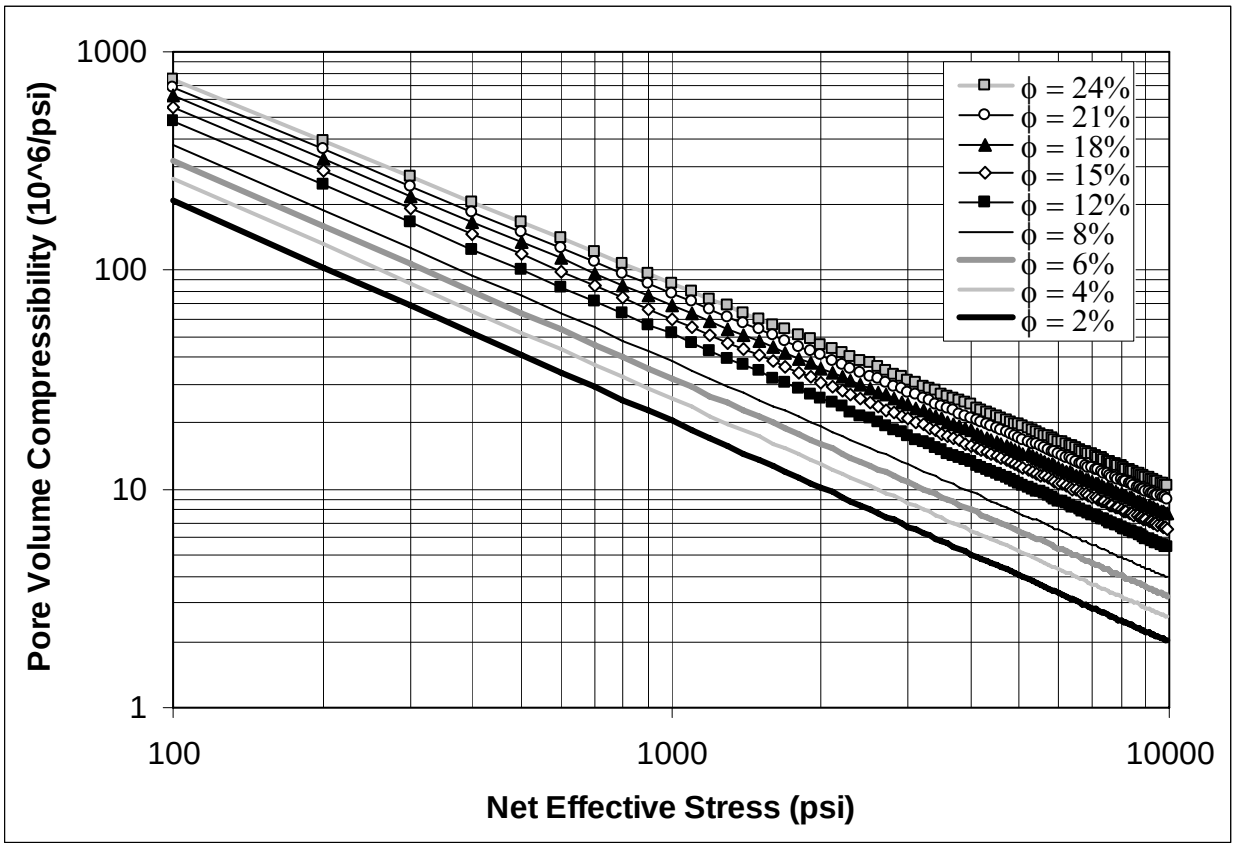

Figure 10. Pore volume compressibility versus net effective stress for Mesaverde sandstones of various porosity as predicted using equation 2 in text.

Compressibilities predicted using equation 2 are generally consistent with values published in the literature (e.g., Jones and Owens, 1981) for individual samples, usually at a given net effective stress. It is important to note that compressibility increases with decreasing confining stress and with increasing porosity.

Subtask 4.5. Measure geologic and petrologic properties

Thin section preparation of low-permeability sandstones has always been hampered by the inability to efficiently impregnate sandstone samples with blue dye epoxy because of the low permeability and the consequent inability to flow epoxy deeply enough into the sample. Most commercial epoxies have an approximate viscosity of 100 centipoise (cp) and a pot life (the time for which the epoxy is liquid before viscosity increases by orders of magnitude) of approximately 30 minutes. To maximize impregnation many techniques have been developed, most notably high pressure impregnation. The depth of penetration is a function of the driving pressure, the pressure in the pores of the sample, the permeability, epoxy viscosity, and capillary forces if epoxy wets the surface. Table 2 illustrates the theoretical depth of penetration of a 100 cp viscosity epoxy into billets of 12.5 mm thickness with application of standard atmospheric pressure into a sample initially evacuated by vacuum. These calculations indicate that for the

standard pot life of 30 minutes (1800 seconds), epoxy penetrates less than 0.27 mm into rocks of less than 0.1 mD. This would indicate that for most low-permeability sandstones the standard impregnation technique does not prove thin sections with blue dye epoxy in the pore space. Even with high-pressure impregnation, where conventionally the samples are placed in a gas pressure vessel an exposed to a gas pressure over the epoxy covering the sample of approximately 1,500 psi (10.3 MPa), impregnation is less than 1 mm for samples with permeability less than 0.01 mD (Table 2).

To improve impregnation efficiency and depth experiments using long pot-life epoxy and pressure were conducted with Zach Wenz of the University of Kansas, Department of Geology. Experiments on Mesaverde sandstone samples found that good impregnation was achieved using an extended pot-life viscosity with moderate pressure. The optimum methodology involved the following steps: 1) cut sandstone billets not greater than 1 cm in thickness to allow efficient evacuation prior to epoxy immersion, 2) grind billet face flat prior to impregnation, 3) evacuate sample to $< 10^{-3}$ torr vacuum, 4) pour extended pot-life epoxy over sample while still under vacuum insuring that sample is completely immersed under epoxy, 5) release vacuum, 6) place samples in high pressure vessel, 7) pressuring vessel to approximately 100-150 psi (700-1000 kPa), 8) leave samples under pressure until epoxy sets or becomes very viscous (e.g., 8-16 hours). An effective 10-hour pot-life viscosity that worked well for the Mesaverde sandstones studied is EPO-TEK 301-2FL®, which is similar to EPO-TEK 301 ® epoxy that is commonly used in thin-section preparation. Table 2 illustrates the approximate depth of penetration for a 100 cp extended pot-life epoxy.

Table 2. epoxy impregnation into 12.5 mm thick sample, ϕ = 10%, with 100 cp viscosity epoxy for various impregnation pressures, sample permeabilities, and time of impregnation. Note that standard pot-life epoxies have pot-life of 30 minutes and impregnation effectively stops at this time and corresponding depth. Orange < 0.1 mm, tan 0.1-1mm, white 1-10mm, blue >10mm penetration depth.

Applied Pressure psi	Capillary force psi	Total pressure psi	Permeablility mD	Epoxy Impregnation Depth (mm) time (min) 2	time (min) 4	time (min) 8	time (min) 10	time (min) 20	time (min) 30	time (min) 300	time (min) 600
14.7	0.3	15	1000	1.25E+01	1.25E+01	1.25E+01	1.25E+01	1.25E+01	1.25E+01	1.25E+01	1.25E+01
14.7	0.7	15	100	1.01E+01	1.25E+01	1.25E+01	1.25E+01	1.25E+01	1.25E+01	1.25E+01	1.25E+01
14.7	1.9	17	10	1.08E+00	2.17E+00	4.33E+00	5.41E+00	1.08E+01	1.25E+01	1.25E+01	1.25E+01
14.7	4.9	20	1	1.28E-01	2.57E-01	5.13E-01	6.41E-01	1.28E+00	1.92E+00	1.25E+01	1.25E+01
14.7	13.0	28	0.1	1.81E-02	3.62E-02	7.23E-02	9.04E-02	1.81E-01	2.71E-01	2.71E+00	5.43E+00
14.7	17.4	32	0.05	1.05E-02	2.10E-02	4.19E-02	5.24E-02	1.05E-01	1.57E-01	1.57E+00	3.14E+00
14.7	34.2	49	0.01	3.19E-03	6.38E-03	1.28E-02	1.60E-02	3.19E-02	4.79E-02	4.79E-01	9.58E-01
14.7	45.7	60	0.005	1.97E-03	3.95E-03	7.89E-03	9.87E-03	1.97E-02	2.96E-02	2.96E-01	5.92E-01
14.7	89.9	105	0.001	6.83E-04	1.37E-03	2.73E-03	3.42E-03	6.83E-03	1.02E-02	1.02E-01	2.05E-01
14.7	120.3	135	0.0005	4.41E-04	8.81E-04	1.76E-03	2.20E-03	4.41E-03	6.61E-03	6.61E-02	1.32E-01
147	0.3	147	1000	1.25E+01	1.25E+01	1.25E+01	1.25E+01	1.25E+01	1.25E+01	1.25E+01	1.25E+01
147	0.7	148	100	1.25E+01	1.25E+01	1.25E+01	1.25E+01	1.25E+01	1.25E+01	1.25E+01	1.25E+01
147	1.9	149	10	9.72E+00	1.25E+01	1.25E+01	1.25E+01	1.25E+01	1.25E+01	1.25E+01	1.25E+01
147	4.9	152	1	9.92E-01	1.98E+00	3.97E+00	4.96E+00	9.92E+00	1.25E+01	1.25E+01	1.25E+01
147	13.0	160	0.1	1.04E-01	2.09E-01	4.18E-01	5.22E-01	1.04E+00	1.57E+00	1.25E+01	1.25E+01
147	17.4	164	0.05	5.37E-02	1.07E-01	2.15E-01	2.68E-01	5.37E-01	8.05E-01	8.05E+00	1.61E+01
147	34.2	181	0.01	1.18E-02	2.37E-02	4.73E-02	5.92E-02	1.18E-01	1.77E-01	1.77E+00	3.55E+00
147	45.7	193	0.005	6.29E-03	1.26E-02	2.52E-02	3.15E-02	6.29E-02	9.44E-02	9.44E-01	1.89E+00
147	89.9	237	0.001	1.55E-03	3.09E-03	6.19E-03	7.74E-03	1.55E-02	2.32E-02	2.32E-01	4.64E-01
147	120.3	267	0.0005	8.73E-04	1.75E-03	3.49E-03	4.36E-03	8.73E-03	1.31E-02	1.31E-01	2.62E-01
1470	0.3	1470	1000	1.25E+01	1.25E+01	1.25E+01	1.25E+01	1.25E+01	1.25E+01	1.25E+01	1.25E+01
1470	0.7	1471	100	1.25E+01	1.25E+01	1.25E+01	1.25E+01	1.25E+01	1.25E+01	1.25E+01	1.25E+01
1470	1.9	1472	10	1.25E+01	1.25E+01	1.25E+01	1.25E+01	1.25E+01	1.25E+01	1.25E+01	1.25E+01
1470	4.9	1475	1	9.63E+00	1.25E+01	1.25E+01	1.25E+01	1.25E+01	1.25E+01	1.25E+01	1.25E+01
1470	13.0	1483	0.1	9.68E-01	1.94E+00	3.87E+00	4.84E+00	9.68E+00	1.25E+01	1.25E+01	1.25E+01
1470	17.4	1487	0.05	4.86E-01	9.71E-01	1.94E+00	2.43E+00	4.86E+00	7.29E+00	1.25E+01	1.25E+01
1470	34.2	1504	0.01	9.82E-02	1.96E-01	3.93E-01	4.91E-01	9.82E-01	1.47E+00	1.25E+01	1.25E+01
1470	45.7	1516	0.005	4.95E-02	9.90E-02	1.98E-01	2.47E-01	4.95E-01	7.42E-01	7.42E+00	1.48E+01
1470	89.9	1560	0.001	1.02E-02	2.04E-02	4.07E-02	5.09E-02	1.02E-01	1.53E-01	1.53E+00	3.06E+00
1470	120.3	1590	0.0005	5.19E-03	1.04E-02	2.08E-02	2.60E-02	5.19E-02	7.79E-02	7.79E-01	1.56E+00
				Standard Pot-life						Extended Pot-life	

CONCLUSIONS

The first public hysteresis capillary pressure curves and measurements of residual nonwetting phase saturation for Mesaverde sandstones are complete and analysis provided parameters for developing a Land-type equation for predicting residual trapped gas saturation in these rocks. The largest and most comprehensive compressibility database for Mesaverde sandstone is also complete and provided the basis for development of an equation that predicts pore volume compressibility for any porosity Mesaverde sandstone at any given net effective confining stress. Confined mercury capillary pressure measurements are preceding smoothly but slowly because equilibration times are longer than previously estimated for the lowest-permeability samples. Because of analysis times of greater than 1 day per sample scheduling for this analysis is behind the timetable presented in the Management Plan. Analysis is being performed within the approved budget.

REFERENCES

Jones, F. O., and Owens, W. W., 1981, A laboratory study of low-permeability gas sands: Journal of Petroleum Technology, v. 32, no. 9, p.1631-1640.

Land, C.S., 1971, “Comparison of calculated with experimental imbibition relative permeability,” Soc. Petroleum Engineering Journal (Dec. 1971) p. 419-425.

Ostensen, R. W., 1983, Microcrack permeability in tight gas sandstone: Society of Petroleum Engineering Journal, v. 23, no. 6, p. 919-927.